Open access • Posted Content • DOI:10.1101/2020.11.05.369728

Enrichment of neurodegenerative microglia signature in brain-derived extracellular vesicles isolated from Alzheimer's disease mouse model — Source link

Satoshi Muraoka, Mark P. Jedrychowski, Naotoshi Iwahara, Mohammad Abdullah ...+7 more authors

Institutions: Boston University, Harvard University

Published on: 06 Nov 2020 - bioRxiv (Cold Spring Harbor Laboratory)

Topics: Neurodegeneration, Apolipoprotein E, Amyloid precursor protein and Microglia

Enrichment of neurodegenerative microglia signature in brain-derived extracellular vesicles isolated from Alzheimer's disease mouse model

Satoshi Muraoka[1], Mark P. Jedrychowski[2], Naotoshi Iwahara[1], Mohammad Abdullah[1], Kristen D. Onos[3], Kelly J. Keezer[3], Jianqiao Hu[1], Seiko Ikezu[1], Gareth R. Howell[3], Steven P. Gygi[2], Tsuneya Ikezu[1,4,5*]

[1]Department of Pharmacology & Experimental Therapeutics, Boston University School of Medicine, Boston, MA, USA; smuraoka@bu.edu (S.M.); niwahara@bu.edu (N.I.); moab@bu.edu (M.A.); lawrenhu@bu.edu (J.H.); sikezu@bu.edu (S.I.)

[2]Department of Cell Biology, Harvard Medical School, Boston, MA, USA; Mark_Jedrychowski@hms.harvard.edu (M.P.J.); steven_gygi@hms.harvard.edu (S.P.G.)

[3]The Jackson Laboratory, Bar Harbor, Maine, ME, USA; Kristen.Onos@jax.org (K.O.); Kelly.keezer@jax.org (K.J.K); Gareth.Howell@jax.org (G.H.)

[4]Department of Neurology, Alzheimer's Disease Center, Boston University School of Medicine, Boston, MA, USA

[5]Center for Systems Neuroscience, Boston University, Boston, MA, USA

[#]**Correspondence author:** Tsuneya Ikezu, MD, PhD

Boston University School of Medicine, 72 East Concord St, L-606B, Boston, MA 02118, USA. Email: tikezu@bu.edu Phone: 617-358-9575 Fax: 617-358-9574

Running title: Protein profiling of CAST.*APP/PS1* mouse brain-derived EVs

25 **Abbreviations**

26 Aβ: Amyloid beta peptide

27 AD: Alzheimer's disease

28 ANXA5: Annexin-5

29 APOE: Apolipoprotein E

30 APP: Amyloid precursor protein

31 BCA: Bicinchoninic acid

32 CNS: Central nervous system

33 CYC1: Cytochrome C

34 DAM/MGnD: disease-associated / neurodegenerative microglia

35 DAVID: Database for annotation, visualization, and integrated discovery

36 DEP: Differentially expressed proteins

37 EVs: Extracellular vesicles

38 FAD: Early-onset / familial AD

39 GM130: 130 kDa cis-Golgi matrix protein

40 HO: Homeostatic microglia

41 ITGAX: Integrin alpha-x

42 LOAD: Sporadic / late-onset AD

43 MS: Mass spectrometry

44 MVBs: Multivesicular bodies

45 NFT: Neurofibrillary tangles

46 NTA: Nanoparticle tracking analysis

47 PS1: Presenilin-1

48 TEM: Transmission electron microscopy

49 TSG101: Tumor susceptibility gene 101 protein

50 UC: Ultracentrifugation

51 TMT: Tandem mass tag

52

53

54

55

56

57

58

59

60

61

62

63

64

65

66

67

68

69

70

Abstract

Extracellular vesicles (EVs) are secreted by any neuronal cells in the central nervous system (CNS) for molecular clearance, cellular communications and disease spread in multiple neurodegenerative diseases, including Alzheimer's disease (AD), although their exact molecular mechanism is poorly understood. We hypothesize that high-resolution proteomic profiling of EVs separated from animal models of AD would determine the composition of EV contents and their cellular origin. Here, we examined recently developed transgenic mice (CAST.*APP/PS1*), which express familial AD-linked mutations of amyloid precursor protein (*APP*) and presenilin-1 (*PS1*) in the CAST/EiJ mouse strain and develop hippocampal neurodegeneration. Quantitative proteomics analysis of EVs separated from CAST.*APP/PS1* and age-matched control mice by tandem mass tag-mass spectrometry identified a total of 3,444 unique proteins, which are enriched in neuron, astrocyte, oligodendrocyte and microglia-specific molecules. CAST.*APP/PS1*-derived EVs show significant enrichment of Psen1, APP, Itgax, and reduction of Wdr61, Pmpca, Aldh1a2, Calu, Anp32b, Actn4 and Ndufv2 compared to WT-derived EVs, suggesting the involvement of Aβ-processing complex and disease-associated / neurodegenerative microglia (DAM/MGnD) in EV secretion. In addition, Itgax and Apoe, the DAM/MGnD markers, in EV show a positive correlation with *Itgax* and *Apoe* mRNA expression from brain tissue in CAST.*APP/PS1* mice. These datasets indicate the significant contribution of Aβ plaque and neurodegeneration-induced DAM/MGnD microglia for EV secretion in CAST.*APP/PS1* mice and shed light on understanding the AD pathogenesis.

Keywords: Alzheimer's disease, amyloid-β peptide, amyloid precursor protein, apolipoprotein E, extracellular vesicles, integrin, microglia, presenilin-1, proteome

Introduction

Alzheimer's disease (AD) is a progressive neurodegenerative disorder and the most common forms of adult dementia affecting 50 million people worldwide (1). The neuropathology of AD is characterized by extracellular deposition of amyloid-β (Aβ) plaques, which are processed by amyloid precursor protein (APP) and presenilin-1 (PS1)-dependent gamma secretase complex, and intraneuronal accumulation of neurofibrillary tangles (NFTs), which are consisted with hyperphosphorylated microtubule-associated protein tau (2-4). There are two form of AD, early-onset / familial AD (FAD) and sporadic / late-onset AD (LOAD) (5, 6). FAD is mostly caused by mutations in *APP* and *PSEN1* and *PSEN2* (7). The FAD mouse models expressing FAD-linked mutation of *APP, PSEN1* or both, have been extensively used to understand the pathophysiology of Aβ deposition although most of them do not develop neurodegeneration (8-10). Onos *et al.* have recently reported a comprehensive assessment of the transgene expression of FAD-linked mutation of *APP* and *PSEN1* in different genetic backgrounds including B6, WSB/EiJ, PWK/PhJ, and CAST/EiJ to establish more clinically-relevant AD mouse models (11). The study showed that CAST.*APP/PS1* line develops reduction in the number of hippocampal pyramidal neurons and robust neuroinflammatory response than previous models (11), which would be more suitable for the assessment of Aβ deposition-induced inflammatory reaction and neuronal cell loss.

Extracellular vesicles (EVs), including exosomes (50-150nm), ectosomes/microvesicles (150-1000nm), and apoptotic bodies (1000-5000nm) are released from almost any neuronal cells (12-14). These EVs contain proteins, mRNA, non-coding RNAs (such as microRNA) and lipids, can transfer these molecules from cells to cells, and can be transported to biofluids, such as and cerebrospinal fluid and blood. In the central nervous system (CNS), brain-derived EVs contain

multiple AD-associated proteins such as Aβ, α-synuclein, APP, cyclin-dependent kinase 5, PSEN1, and tau, and play important roles in Aβ deposition and tauopathy (15-20). Moreover, it has been reported that inhibition of EV synthesis reduced Aβ plaque deposition in the mouse model of AD, and stimulation of EV secretion increased intracellular transfer of prion protein in AD mouse models (16, 17). EVs are involved in the extracellular enzymatic degradation of Aβ and promote both Aβ aggregation and clearance by microglia (18, 19), although their exact molecular mechanism is poorly understood. We hypothesize that high-resolution proteomic profiling of EVs separated from animal models of AD would determine the composition of EV contents and their cellular origin. Here we provide the quantitative proteomics profiling of EVs separated from CAST.*APP/PS1* transgenic mouse brain tissue and show brain-derived EV molecules altered during early-onset AD.

Materials and methods

CAST.-*APP/PS1* transgenic mouse model

The CAST.-*APP/PS1* transgenic mouse line, which expresses human APP^{swe} and $PS1^{de9}$, was created in the Howell lab colony at The Jackson Laboratory by backcrossing for at least seven generations the *APP/PS1* transgenes from C57BL/6J (B6) to CAST (11). Brain samples (forebrain and hindbrain) were extracted from 6 female CAST.*APP/PS1* and 6 female CAST (WT) littermate control mice at 8 months of age. Mice were anesthetized with ketamine/xylazine prior to tissue harvest.

Brain tissue homogenates

Frozen whole brain tissue was chopped on ice using a razor blade (# 12-640 Fischer Scientific) to generate approximately 0.5 mm-wide pieces, and homogenized by a sonicator. The homogenized tissue was lyzed using Guanidine Hydrochloride (# 50950-250G Sigma).

Separation of EVs from mouse brain tissue

Brain tissue (0.4 g per sample) was processed for EV extraction based on our reported method with modifications. Briefly, frozen whole brain tissue was chopped on ice using a razor blade (# 12-640 Fischer Scientific) to generate approximately 0.5 mm-wide pieces. The sections were transferred to 3mL of Hibernate E solution (# A1247601 Gibco) containing 20 U of papain (# LK003178 Worthington-biochemical corporation) in Earle's Balanced Salt Solution (EBSS) (# 14155063 Gibco) and then incubated at 37°C for 15 min by stirring once every 5 min. After the incubation, the samples were placed on ice, and added with 6 mL of ice-cold Hibernate E solution supplemented with Halt™ Protease and Phosphatase Inhibitor Cocktails (# PI78443 Fisher scientific). The samples were gently homogenized (20 strokes) with a glass-Teflon homogenizer (# 89026-384 VWR), and filtered with 40-µm mesh filter (# 22-363-547 Fisher scientific), followed by centrifugation at 300 × *g* for 10 min at 4°C (# 5720R Eppendorf). The supernatant was transferred to a new 15-mL polypropylene tube and centrifuged at 2,000 × *g* for 10 min at 4°C (# 5720R Eppendorf). The supernatant was transferred to a 30-mL conical tube and centrifuged at 10,000 × *g* for 10 min at 4°C (#5424R Eppendorf). The supernatant filtered through a 0.22-µm polyethersulfone membrane filter (# SLGP033RS EMD Millipore) into new a polyallomer ultracentrifuge tube with 13.2-mL capacity (# 331372 Beckman Coulter), diluted with double-filtered phosphate-buffered saline (dfPBS) with 0.22-µm polyethersulfone membrane filter to 12 mL, and centrifuged at 140,000 × *g* for 70 min at 4°C (# Optima-XE SW41 Beckman Coulter). The pellet was resuspended in 2 mL of 0.475M of sucrose solution (#

S5-3 Fisher science) in dfPBS. The sucrose step gradient was created in dfPBS with six 2-mL steps starting from 2.0M to 1.5M, 1.0M, 0.825M, 0.65M, and 0.475M (containing the resuspended pellet) in a polyallomer ultracentrifuge tube. The gradient was centrifuged at 200,000 × *g* for 20 h at 4°C (35,000 rpm with # Optima-XE SW41 Beckman Coulter). The gradient was collected in 2-mL fractions, except for the first and last fractions, which were 1 mL each. The interphases between the second (0.65M) and third (0.825M) steps correspond to fraction "V" and the third and fourth steps corresponded to fraction "VI" have a buoyant density of 1.10 - 1.12 and 1.12 - 1.15 g/cm^3, respectively, and enriched in EVs. The V and VI fractions were diluted to a total volume of 12 mL with dfPBS and centrifuged at 140,000 × *g* for 70 min at 4°C (# Optima-XE SW41 Beckman Coulter), and each pellet were resuspend with 30 µl of dfPBS. The fraction V and VI fractions were mixed as an EV-enriched sample.

Protein concentrations

The bicinchoninic acid (BCA) assay was used to determine protein concentration for each sample using BCA protein assay kit (# 23225 Pierce) as previously described (21). EVs were diluted 1:10 before loading into the assay, and a 1:8 ratio of sample to reaction components was used. All assays were allowed to incubate at 37°C for 30 min before protein concentration was read in at 562 nm (SynergyMix, Biotek).

Nanoparticle Tracking Analysis (NTA)

All samples were diluted in dfPBS at least 1:8000 to get particles within the target reading range for the Nanosight 300 machine (Malvern Panalytical Inc), which is 10-100 particles per frame. Using a manual injection system, four 60-s videos were taken for each sample at 21°C. Analysis of particle counts was carried out in the Nanosight NTA 3.2 software (Malvern Panalytical Inc) with a detection threshold of 5.

Transmission electron microscopy (TEM)

The EV separated from *APP/PS1* and control mouse brain tissue were analyzed by TEM. The EV sample (5µl) was adsorbed for 1 min to a carbon-coated mesh grid (# CF400-CU, Electron Microscopy Sciences) that had been made hydrophilic by a 20-s exposure to a glow discharge (25 mA). Excess liquid was removed with a filter paper (# 1 Whatman). The grid was then floated briefly on a drop of water (to wash away phosphate or salt), blotted on a filer paper, and then stained with 0.75% uranyl formate (# 22451 Electron Microscopy Sciences) for 30 s. After removing the excess uranyl formate, the grids were examined, and random fields were photographed using a JEOL 1200EX TEM with an AMT 2k CCD camera at the Electron Microscopy Facility, Harvard Medical School, Boston, MA.

Western blotting

EV samples and brain tissue homogenate samples were run in a 4% to 20% gradient gel (# 4561093 Bio-Rad) and electro-transferred to Immobilon-P membrane, PVDF 0.45-µm (# 10344661 Fisher scientific). The membrane was blocked in freshly prepared 5% BSA diluted in TBS before being immunoblotted with specific primary antibodies (CD81; #EXOAB-CD81A-1 System Biosciences, GM130; #610822 Becton Dickinson, Cytochrome C; #11940T Cell Signaling Technology, ANXA5, ItgaX; #14-011485 eBioscience) or HRP-labeled primary antibodies (TSG101; # SC-7964 Santa Cruz Biotechnology). The membrane was incubated with HRP-labeled secondary antibodies (Santa Cruz Biotechnology) and scanned using the C300 digital chemiluminescent imager (Azure Biosystems).

High-Resolution Liquid Chromatography-Tandem Mass-tag Mass spectrometry

SDS-PAGE and In-gel digestion

Ice-cold 100% (w / v) trichloroacetic acid (TCA) (# T6399 Sigma-Aldrich) was added to the separated EV fraction to a final concentration of 20% of TCA, then the mixed sample was incubated for 30 min on ice and was centrifuged at 15,000 g for 20 min at 4°C. The pellet was then washed twice with ice-cold acetone (# 179124 Sigma-Aldrich). After drying, the pellet was resuspended in Laemmli sample buffer (# 1610747 Bio-Rad) with 5 mM dithiothreitol (# 43815 Sigma-Aldrich), reduced for 20 min at 65°C, and alkylated with 15 mM iodoacetamide (# I1149 Sigma-Aldrich) for 20 min at room temperature in the dark. Subsequently, the samples were run in a 4% to 20% gradient gel (# 4561096 Bio-Rad) until the dye front was 10 mm from the top of the gel. The gels were washed twice with distilled water, fixed with 100% Methanol, and stained with GelCode Blue Stain Reagent (# 24590 Thermo Fisher Scientific) for 16 hrs. Each lane was then individually removed from the gel. Gel pieces were then transferred to 1.5 mL tubes and destained twice using 50% acetonitrile (J. T. Baker, USA) in 25 mM HEPES (pH 8.8) at 22°C, for 15 min with shaking, and dehydrated with 100% acetonitrile for additional 10 min with shaking, for a total of three times. The destained gel piece was dried up using SpeedVac Concentrators (Thermo Fisher Scientific). The gel pieces were digested with proteomic grade trypsin (# 03708985 Roche, USA) in 25 mM HEPES overnight at 37°C. The digested peptide was extracted with 70% acetonitrile /1% formic acid, and were removed the gel by Ultrafree-MC Centrifugal Filter (# UFC30L Millipore USA). The digested peptides were reconstituted in 25 µL of 200 mM EPPS (pH 8.0) and vortexed for 5 min.

Peptide labeling with TMT 16-plex isobaric labeling Kit

Tandem mass tag (TMT) labeling was performed according to manufacturer's instructions (# A44520 Thermo Fisher Scientific). In brief, 4 µL of TMT Label reagent (20 ng/µL) was added to the digested peptides in 30 µL of 200 mM HEPPS (4-(2-Hydroxyethyl)-1-

piperazinepropanesulfonic acid), pH8.0. After incubation at room temperature for 1 h, the reaction was quenched with 2 µL of 5% hydroxylamine in water for 15min. The TMT-labeled peptide samples were pooled at a 1:1 ratio across ten samples. The combined sample was added to 100 µL of 20% formic acid, 2 mL of 1% formic acid, desalted via StageTip, dried by vacuum centrifugation, and resuspended in 20 µL of 5% acetonitrile and 5% formic acid for nano liquid chromatography and tandem mass-spectrometry (Nano LC-MS/MS/MS).

Nano-Liquid Chromatography and Tandem Mass-tag Spectrometry (LC-MS/MS/MS)

Nano LC–MS/MS/MS analysis was conducted using an LTQ-Orbitrap Fusion Lumos mass spectrometer (Thermo Fisher Scientific, USA) equipped with a Proxeon EASY-nano LC 1200 liquid chromatography pump (Thermo Fisher Scientific, San Jose, CA). Peptides were separated on a 100 µm inner diameter microcapillary column packed with 35-cm long Accucore150 resin (2.6 µm, 150 Å, Thermo Fisher Scientific). We loaded 4 µL onto the column and separation was achieved using a 180 min gradient of 8 to 23% acetonitrile in 0.125% formic acid at a flow rate of ~550 nL/min. The analysis used an MS^3 based TMT method, which has been shown to reduce ion interference. The scan sequence began with an MS1 spectrum (Orbitrap; resolution 120,000; mass range 400-1400m/z; automatic gain control (AGC) target 5×10^5; maximum injection time 100ms). Precursors for MS^2/MS^3 analysis were selected using a Top10 method. MS2 analysis consisted of collision-induced dissociation (quadrupole ion trap; AGC 2×10^4; normalized collision energy (NCE) 35; maximum injection time 150ms). Following acquisition of each MS^2 spectrum, we collected an MS^3 spectrum using our recently described method in which multiple MS^2 fragment ions were captured in the MS^3 precursor population using isolation waveforms with multiple frequency notches (22). MS^3 precursors were fragmented by high-energy collision-

induced dissociation (HCD) and analyzed using the Orbitrap (NCE 65; AGC 1×10^5; maximum injection time 150ms, resolution was 50,000 at 200Th).

Mass-spectrometry data analysis

A compendium of in-house developed software was used to convert mass spectrometric data (Raw file) to the mzXML format, as well as to correct monoisotopic m/z measurements (23). Database searching included all entries from the *Mus musculus* with human APP and PS1 UniProt database (ver. October 2018). This database was concatenated with one composed of all protein sequences in the reversed order. Searches were performed using a 50ppm precursor ion tolerance for total protein level profiling (22). The product ion tolerance was set to 0.9 Da, which was chosen to maximize sensitivity in conjunction with SEQUEST searches and linear discriminant analysis. TMT tags on lysine residues and peptide N termini (+229.163 Da) and carbamidomethylation of cysteine residues (+57.021 Da) were set as static modifications, while oxidation of methionine residues (+15.995 Da) was set as a variable modification. Peptide-spectrum matches (PSMs) were adjusted to a 1% false discovery rate (FDR). Filtering was performed using an in-house linear discrimination analysis (LDA) method to create one combined filter parameter from the following peptide ion and MS^2 spectra metrics: SEQUEST parameters XCorr and ΔCn, peptide ion mass accuracy and charge state, in-solution charge of peptide, peptide length, and mis-cleavages. Linear discrimination scores were used to assign probabilities to each MS^2 spectrum for being assigned correctly, and these probabilities were further used to filter the dataset with an MS^2 spectra assignment FDR of smaller than 1% at the protein level (24). For TMT-based reporter ion quantitation, we extracted the summed signal-to-noise (S/N) ratio for each TMT channel and found the closest matching centroid to the expected mass of the TMT reporter ion. PSMs were identified, quantified, and collapsed to a 1% peptide

FDR and then collapsed further to a final protein-level FDR of 1%. Moreover, protein assembly was guided by principles of parsimony to produce the smallest set of proteins necessary to account for all observed peptides. Proteins were quantified by summing reporter ion counts across all matching PSMs. PSMs with poor quality, MS^3 spectra with more than eight TMT reporter ion channels missing, MS^3 spectra with TMT reporter summed signal-to-noise ratio less than 100, or no MS^3 spectra were excluded from quantification (25). The mass spectrometry proteomics data have been deposited to the ProteomeXchange Consortium via the PRIDE partner repository (26) with the dataset identifier PXD022349. Protein quantitation values were exported for further analysis in Microsoft Excel or Prism8. Each reporter ion channel was summed across all quantified proteins.

Experimental design and statistical analysis

EVs were isolated from brain tissue of 6 female CAST.*APP/PS1* and 6 female CAST (WT) littermate control mice at 8 months of age. Statistical analysis was conducted using Prism 8 (GraphPad, Inc.). Between group comparisons were analyzed by Welch's t-test. The Gene Ontology of identified proteins were elucidated by the Database for Annotation, Visualization and Integrated Discovery (DAVID) Bioinformatics Resources 6.8. The venn diagram and heatmap analysis were generated using Venny_2.1 (http://bioinfogp.cnb.csic.es/tools/venny/) and ClustVis (https://biit.cs.ut.ee/clustvis/).

Results

Biochemical and morphological characterization of EVs separated from brain tissue

We separated EVs from mouse brain tissues by ultracentrifugation and sucrose gradient ultracentrifugation as previously described (21). To check the purity of the EV preparation from

297 mouse brain tissues, the EV fractions were analyzed for their size and number by NTA. The EV
298 fractions were enriched the particle of small size (median 122 nm) compared to brain
299 homogenate (median 165 nm, **Figure 1A**). The particles per protein were 2.08×10^7 [particles /
300 μg] in brain homogenate and 1.40×10^9 [particles / μg] in separated EV fraction (**Figure 1B**),
301 showing significant enrichment ($p < 0.001$). The EV markers such as Tumor susceptibility gene
302 101 protein (TSG101) and CD81 were clearly represented in EV fractions, whereas
303 contamination markers such as 130 kDa cis-Golgi matrix protein (GM130) and cytochrome C
304 (CYC1) in MISEV2018 guidelines (12) were absent in the EV fraction (**Figure 1C**). The
305 separated EVs were examined by transmission electron microscopy (TEM), which shows cap-
306 shaped morphology as commonly seen separated EVs (**Figure 1D**). These data demonstrate the
307 successful enrichment of EV fraction from mouse brain tissues.

308 **Proteomic profiling of EVs from CAST.*APP/PS1* and WT mouse brain tissue**

309 The median diameter of separated EVs was 120 nm for WT and 112 nm for *APP/PS1* groups,
310 and the particle counts were 7.03×10^{11} particles for WT and 1.38×10^{12} particles for *APP/PS1*
311 groups (**Figure 2A**). There were no significantly difference in these parameters between WT and
312 *APP/PS1* groups (Diameter: $p = 0.4848$, particle counts: $p = 0.0649$). We next analyzed the
313 protein profiles of EVs separated from *APP/PS1* and WT mouse brain tissues by LC-MS/MS/MS
314 using TMT-based labeling (27). We identified a total of 3444 unique proteins **(Supplementary**
315 **Table S1 and S2)**. The identified proteins were compared with the top 100 EV proteins from the
316 ExoCarta database (28). The Venn diagram represents 90 of the top 100 EV proteins commonly
317 found in the mouse brain-derived EVs **(Figure 2B)**. We analyzed the proteomic dataset using
318 Database for Annotation, Visualization, and Integrated Discovery (DAVID Gene Ontology
319 (GO)) (29, 30). The identified proteins show significantly enrichment of extracellular exosome

by 'cellular component', and transport and protein-binding molecules by 'Biological process' and 'Molecular function', respectively (**Figure 2C**). The KEGG pathway analysis showed enrichment of endocytosis and glutamatergic synapse molecules, which are related to microglia and neuronal functions. The EV proteins were mostly annotated brain, brain cortex and hippocampus by Tissue ontology as expected **(Figure 2C)**. Taken together, these results show successful enrichment of proteins specific to EVs, cadherin/protein binding molecules, neuronal /glial functions and brain tissues in separated EV samples.

Neural cell-type specific proteins of EVs derived from mouse brain tissue

We next examined the enrichment of neural cell-type specific molecules in the EV proteomic dataset using the proteomic dataset of neural cells, such as neurons, astrocytes, microglia and oligodendrocytes separated from mouse brain tissues by a bio-panning method as a reference (31). The identified neural cell-type specific markers (155 total) are 43.9 % (68) neurons, 5.8% (9) microglia, 27.1% (42) astrocytes and 23.2% (36) oligodendrocytes **(Figure 3A)**. We examined the changes in the expression of these cell type-specific markers in EVs separated from *APP/PS1* and WT groups. The neuron-specific molecules downregulated in *APP/PS1* compared to WT include Pclo (Piccolo), Add2 (Beta-adducin), L1cam (Neural cell adhesion molecule L1), Calb2 (Calretinin) and Calb1 (Calbindin), while upregulated molecules include Camkv (CaM kinase-like vesicle-associated protein), Gprin1 (G protein-regulated inducer of neurite outgrowth 1), Ngef (Ephexin-1), and Fxyd6 (FXYD domain-containing ion transport regulator 6) (**Figure 3B**). The astrocyte-specific molecules downregulated in *APP/PS1* compared to WT include Aldh1a2 (Retinal dehydrogenase 2), Nid1 (Nidogen-1), Lamb2 (Laminin subunit beta-2) and Cbs (Cystathionine beta-synthase), while upregulated molecules include Sorbs1 (Sorbin and SH3 domain-containing protein 1), Fmn2 (Formin-2) and Pacsin3 (Protein kinase C

and casein kinase II substrate protein 3). The oligodendrocyte-specific molecules downregulated in *APP/PS1* compared to WT include P4ha1 (Prolyl 4-hydroxylase subunit alpha-1), Mog (Myelin-oligodendrocyte glycoprotein), Tnr (Tenascin-R) and Hmgcs1 (Hydroxymethylglutaryl-CoA synthase, cytoplasmic), while upregulated molecules include Col1a1 (Collagen alpha-1(I) chain), Pde9a (High affinity cGMP-specific 3',5'-cyclic phosphodiesterase 9A) and Cnp (C-type natriuretic peptide). There are limited changes in the microglia-specific molecules identified by the previous proteomic study. To compensate the information, we have used the microglia-specific gene signature identified from microglia separated from another *APP/PS1* mouse models (32-34), namely disease-associated/neurodegenerative microglia (DAM/MGnD) and homeostatic microglia (HO). We identified DAM/MGnD-specific molecules, especially integrin alpha-x (Itgax) and apolipoprotein E (Apoe) upregulated in EVs from *APP/PS1* compared to WT group as determined by the scattered plot analysis of Log_2 fold changes of EV proteomic dataset and the microglia gene expression profile (**Figure 3C**). These data indicate global changes in the contribution of EV production in different neural cell types, suggesting their potential application in monitoring the disease progression and understanding the pathobiology.

Comparison of *APP/PS1* and WT mouse brain-derived EV proteins by TMT-labeling proteomics analysis

We analyzed the fold change and *p*-values of proteins by Volcano plot, which shows that 3 proteins were significantly upregulated ($p < 0.05$, $Log_2FC > 0.585$ or < -0.5585) , while 7 proteins were significantly down-regulated in *APP/PS1* compared to the WT **(Figure 4A)**. The three significantly upregulated molecules are Psen1, App and Itgax (**Figure 4B**). Among them, Psen1 and App are likely due to their transgene expression in *APP/PS1* mice, thus Itgax (CD11c), which is the most representative marker of DAM/MGnD, is the only endogenous

366 molecule significantly upregulated in the separated EVs from *APP/PS1* mouse brain. The seven
367 significantly downregulated molecules are WD repeat-containing protein 61 (Wdr61),
368 Mitochondrial-processing peptidase subunit alpha (Pmpca), Retinal dehydrogenase 2 (Aldh1a2,
369 also astrocyte-specific marker), Calumenin (Calu), Acidic leucine-rich nuclear phosphoprotein
370 32 family member B (Anp32b), Alpha-actinin-4 (Actn4), and NADH dehydrogenase
371 flavoprotein 2 (Ndufv2) **(Figure 4C)**. The 46 significantly differentially expressed proteins
372 (DEPs, $p < 0.05$) are displayed in a heatmap, showing two clusters either upregulated or
373 downregulated in *APP/PS1* compared to WT group **(Figure 4D)**. The upregulated proteins
374 include Anxa5 (Annexin-5), which specifically binds to the phosphatidylserine expressed on
375 dying cells (35). We recently reported ANXA5 as the most upregulated molecules in AD brain-
376 derived EVs compared to healthy control group (20). We also confirmed the expression of
377 ANXA5 by immunoblotting of EVs separated from *APP/PS1* and WT mouse brains
378 **(Supplementary Figure. S1)**. We compared the ratio of mRNA levels in *APP/PS1* mouse brain
379 tissues over WT controls, which was published (11) and the ratio protein levels EVs separated
380 from *APP/PS1* mouse brains over WT controls in this study by a scattered plot (**Figure 4E**). The
381 Itgax protein show highly positive correlation with Itgax mRNA level ($\log_2$ mRNA expression
382 ratio; 3.77, $\log_2$ EV protein expression ratio; 1.44). These data demonstrate that DAM/MGnD
383 induction in *APP/PS1* mouse brain, as determined by Itgax expression, may contribute to the
384 enhanced EV production by microglia, which is shown in the upregulation of Itgax in *APP/PS1*
385 mouse brain-derived EVs. The ItgaX protein was upregulated in EVs separated from *APP/PS1*
386 mouse brains using immunoblotting **(Figure 4F)**.
387
388 **Discussion**

In the present study, we separated EVs from brain tissue of CAST.*APP/PS1* transgenic mice and age-matched CAST WT littermates. The EV samples were biophysically and morphologically characterized and subjected TMT-labeled high-resolution quantitative proteomic profiling by Nano LC-MS/MS/MS. A total of 3,444 unique proteins from brain-derived EVs, were found to be enriched as extracellular exosomes molecules. The identified EV proteins were enriched in neural cell type and DAM/MGnD -specific molecules in CAST.*APP/PS1* compared to WT group. Itgax, the DAM/MGnD marker, was significantly upregulated in EVs from CAST.*APP/PS1* compared to WT mouse brains. In addition, the significantly increased level of ANXA5 in the CAST.*APP/PS1* group, which was also increased in AD brain-derived EVs, was confirmed by western blot.

The protein levels of APP and Psen1 were also significantly upregulated in CAST.*APP/PS1* brain-derived EVs compare to WT. The peptides of APP identified in both groups by Nano-LC-MS/MS, which covered 14.5% of APP, including the corresponding amyloid-β peptide region **(Supplementary Figure S2)**. The quantification value of identified peptides, which contain amyloid beta peptide and C-terminal peptide showed to upregulate 1.5 - 2.0 folds in CAST.*APP/PS1* compared to WT in **Supplementary Table S3**. The EV in CAST.*APP/PS1*, therefore, may contain amyloid-β peptide, full-length APP and cleaved C-terminal APP. Our attempt to detect these molecules by ELISA was unsuccessful due to the scarcity of the target molecules (data not shown).

Itgax is a well-established integrin and form complex with Integrin beta2 (Itgb2/CD18) as inactivated-C3b receptor 4 (complement receptor 4) (36). The expression levels of Itgax is specifically increased in DAM/MGnD microglia separated from aged *APP/PS1* mice (37). In addition, we have recently shown that amyloid plaque-associated $Mac2^{+}$ DAM/MGnD microglia

hyper-secrete EVs to extracellular regions in *App*$^{NL-G-F}$ knockin mouse model, demonstrating that DAM/MGnD plays a key role in EV secretion in AD mouse brains (38).

We compare the EV proteomics data to human AD brain-derived EV proteomics data (20), the 380 proteins were common between CAST.*APP/PS1* brain-derived EVs and human AD brain-derived EVs **(Supplementary Figure S3)**. The APOE, CAMKV, ANXA5 and VGF showed a similar correlation with these EVs, suggesting that Aβ deposition may be the major pathology for the upregulation of these molecules in EVs.

The study has some limitation. The first is the limited amount of EVs that can be separated from mouse brain (9.7 - 27.5 μg/whole brain). It is often difficult to detect proteins of interest unless highly sensitive quantification method (such as digital ELISA) is available with the limited amount of proteins. The second is the depth of identified neural cell type-specific molecules from mouse brains that are publicly available. This is especially an issue for microglia-specific markers in this study. This can be compensated by the dataset of cell type-specific gene expression analysis, but these molecules still need to be validated by proteomic approaches. Another issue is the lack of other neuropathology in *APP/PS1* mouse models, such as tau accumulation, cortical atrophy, which may attribute to the difference in proteomic profiles of EVs separated from human and mouse brain tissues. Further studies will be necessary to address these limitations by the use of more robust and sensitive protein detection systems, development of more comprehensive dataset for neural cell type-specific proteome, and application of animal models more closely recapitulating AD progression in brain.

In summary, we have profiled a total of 3,444 proteins in EV samples separated from CAST.*APP/PS1* and CAST WT mouse brain tissues at 8 months of age. *APP/PS1* mouse brain-derived EVs are enriched in App, Psen1, Itgax and Anxa5, representing the amyloid pathology

progression, contribution of DAM/MGnD-derived EVs and apoptotic cell-detecting molecules: A highly relevant molecular set for understanding the disease progression in *APP/PS1* mouse brains.

Acknowledgment

The authors thank M. Ericsson (Electron Microscopy Facility, Harvard Medical School) for electron microscopic imaging services.

Conflict of Interest

The authors declare that the research was conducted in the absence of any commercial or financial relationships that could be construed as a potential conflict of interest.

Author Contributions

S.M. and T.I. designed research; S.M., M.P.J., N.I., M.A., and K.O. performed research; S.M., M.P.J., N.I., J.H., and S.P.G. analyzed data; L.O., and G.H. provided brain sample; and S.M., and T.I. wrote the paper; S.M., W.P.J., N.I., M.A., S.I., and T.I. edited the paper.

Funding

This work is in part funded by Alzheimer's Association AARF-9550302678 (SM), Cure Alzheimer's Fund (TI), NIH R01 AG066429 (TI), NIH RF1 AG054199 (TI), NIH R56 AG057469 (TI), NIH RF1 AG051496 (GRH), NIH RF1 AG055104 (GRH) and BU ADC P30 AG013846 (SI).

References

458 1. Selkoe, D. J., and Hardy, J. (2016) The amyloid hypothesis of Alzheimer's disease at
459 25 years. *EMBO Mol Med* 8, 595–608
460 2. Masters, C. L., Bateman, R., Blennow, K., Rowe, C. C., Sperling, R. A., and Cummings,
461 J. L. (2015) Alzheimer's disease. *Nat Rev Dis Primers* 1, 15056
462 3. Ittner, L. M., and Götz, J. (2011) Amyloid-β and tau--a toxic pas de deux in Alzheimer's
463 disease. *Nat. Rev. Neurosci.* 12, 65–72
464 4. Goedert, M. (2015) NEURODEGENERATION. Alzheimer“s and Parkinson”s diseases:
465 The prion concept in relation to assembled Aβ, tau, and α-synuclein. *Science* 349, 1255555–
466 1255555
467 5. Barber, R. C. (2012) The genetics of Alzheimer's disease. *Scientifica (Cairo)* 2012,
468 246210–14
469 6. Adam, M. P., Ardinger, H. H., Pagon, R. A., Wallace, S. E., Bean, L. J., Stephens, K.,
470 Amemiya, A., and Bird, T. D. (1993) Early-Onset Familial Alzheimer Disease – RETIRED
471 CHAPTER, FOR HISTORICAL REFERENCE ONLY. *PLoS Med* 14, e1002270
472 7. Bertram, L., and Tanzi, R. E. (2008) Thirty years of Alzheimer's disease genetics: the
473 implications of systematic meta-analyses. *Nat. Rev. Neurosci.* 9, 768–778
474 8. Sasaguri, H., Nilsson, P., Hashimoto, S., Nagata, K., Saito, T., De Strooper, B., Hardy, J.,
475 Vassar, R., Winblad, B., and Saido, T. C. (2017) APP mouse models for Alzheimer's disease
476 preclinical studies. *EMBO J.* 36, 2473–2487
477 9. Platt, T. L., Reeves, V. L., and Murphy, M. P. (2013) Transgenic models of Alzheimer's
478 disease: better utilization of existing models through viral transgenesis. *Biochim. Biophys. Acta*
479 1832, 1437–1448

480 10. Balducci, C., and Forloni, G. (2011) APP transgenic mice: their use and limitations.
481 *Neuromolecular Med.* 13, 117–137
482 11. Onos, K. D., Uyar, A., Keezer, K. J., Jackson, H. M., Preuss, C., Acklin, C. J., O'Rourke,
483 R., Buchanan, R., Cossette, T. L., Sukoff Rizzo, S. J., Soto, I., Carter, G. W., and Howell, G. R.
484 (2019) Enhancing face validity of mouse models of Alzheimer's disease with natural genetic
485 variation. *PLoS Genet.* 15, e1008155
486 12. Thery, C., Witwer, K. W., Aikawa, E., Alcaraz, M. J., Anderson, J. D., Andriantsitohaina,
487 R., Antoniou, A., Arab, T., Archer, F., Atkin-Smith, G. K., Ayre, D. C., Bach, J.-M., Bachurski,
488 D., Baharvand, H., Balaj, L., Baldacchino, S., Bauer, N. N., Baxter, A. A., Bebawy, M.,
489 Beckham, C., Bedina Zavec, A., Benmoussa, A., Berardi, A. C., Bergese, P., Bielska, E.,
490 Blenkiron, C., Bobis-Wozowicz, S., Boilard, E., Boireau, W., Bongiovanni, A., Borràs, F. E.,
491 Bosch, S., Boulanger, C. M., Breakefield, X., Breglio, A. M., Brennan, M. Á., Brigstock, D. R.,
492 Brisson, A., Broekman, M. L., Bromberg, J. F., Bryl-Górecka, P., Buch, S., Buck, A. H., Burger,
493 D., Busatto, S., Buschmann, D., Bussolati, B., Buzás, E. I., Byrd, J. B., Camussi, G., Carter, D.
494 R., Caruso, S., Chamley, L. W., Chang, Y.-T., Chen, C., Chen, S., Cheng, L., Chin, A. R.,
495 Clayton, A., Clerici, S. P., Cocks, A., Cocucci, E., Coffey, R. J., Cordeiro-da-Silva, A., Couch,
496 Y., Coumans, F. A., Coyle, B., Crescitelli, R., Criado, M. F., D'Souza-Schorey, C., Das, S., Datta
497 Chaudhuri, A., de Candia, P., De Santana, E. F., De Wever, O., Del Portillo, H. A., Demaret, T.,
498 Deville, S., Devitt, A., Dhondt, B., Di Vizio, D., Dieterich, L. C., Dolo, V., Dominguez Rubio,
499 A. P., Dominici, M., Dourado, M. R., Driedonks, T. A., Duarte, F. V., Duncan, H. M.,
500 Eichenberger, R. M., Ekström, K., Andaloussi, El, S., Elie-Caille, C., Erdbrügger, U., Falcon-
501 Perez, J. M., Fatima, F., Fish, J. E., Flores-Bellver, M., Försönits, A., Frelet-Barrand, A., Fricke,
502 F., Fuhrmann, G., Gabrielsson, S., Gámez-Valero, A., Gardiner, C., Gärtner, K., Gaudin, R.,

503 Gho, Y. S., Giebel, B., Gilbert, C., Gimona, M., Giusti, I., Goberdhan, D. C., Görgens, A.,
504 Gorski, S. M., Greening, D. W., Gross, J. C., Gualerzi, A., Gupta, G. N., Gustafson, D.,
505 Handberg, A., Haraszti, R. A., Harrison, P., Hegyesi, H., Hendrix, A., Hill, A. F., Hochberg, F.
506 H., Hoffmann, K. F., Holder, B., Holthofer, H., Hosseinkhani, B., Hu, G., Huang, Y., Huber, V.,
507 Hunt, S., Ibrahim, A. G.-E., Ikezu, T., Inal, J. M., Isin, M., Ivanova, A., Jackson, H. K.,
508 Jacobsen, S., Jay, S. M., Jayachandran, M., Jenster, G., Jiang, L., Johnson, S. M., Jones, J. C.,
509 Jong, A., Jovanovic-Talisman, T., Jung, S., Kalluri, R., Kano, S.-I., Kaur, S., Kawamura, Y.,
510 Keller, E. T., Khamari, D., Khomyakova, E., Khvorova, A., Kierulf, P., Kim, K. P., Kislinger, T.,
511 Klingeborn, M., Klinke, D. J., Kornek, M., Kosanović, M. M., Kovács, Á. F., Krämer-Albers, E.-
512 M., Krasemann, S., Krause, M., Kurochkin, I. V., Kusuma, G. D., Kuypers, S., Laitinen, S.,
513 Langevin, S. M., Languino, L. R., Lannigan, J., Lässer, C., Laurent, L. C., Lavieu, G., Lázaro-
514 Ibáñez, E., Le Lay, S., Lee, M.-S., Lee, Y. X. F., Lemos, D. S., Lenassi, M., Leszczynska, A., Li,
515 I. T., Liao, K., Libregts, S. F., Ligeti, E., Lim, R., Lim, S. K., Linē, A., Linnemannstöns, K.,
516 Llorente, A., Lombard, C. A., Lorenowicz, M. J., Lörincz, Á. M., Lötvall, J., Lovett, J., Lowry,
517 M. C., Loyer, X., Lu, Q., Lukomska, B., Lunavat, T. R., Maas, S. L., Malhi, H., Marcilla, A.,
518 Mariani, J., Mariscal, J., Martens-Uzunova, E. S., Martin-Jaular, L., Martinez, M. C., Martins, V.
519 R., Mathieu, M., Mathivanan, S., Maugeri, M., McGinnis, L. K., McVey, M. J., Meckes, D. G.,
520 Meehan, K. L., Mertens, I., Minciacchi, V. R., Möller, A., Møller Jørgensen, M., Morales-
521 Kastresana, A., Morhayim, J., Mullier, F., Muraca, M., Musante, L., Mussack, V., Muth, D. C.,
522 Myburgh, K. H., Najrana, T., Nawaz, M., Nazarenko, I., Nejsum, P., Neri, C., Neri, T.,
523 Nieuwland, R., Nimrichter, L., Nolan, J. P., Nolte-'t Hoen, E. N., Noren Hooten, N., O'Driscoll,
524 L., O'Grady, T., O'Loghlen, A., Ochiya, T., Olivier, M., Ortiz, A., Ortiz, L. A., Osteikoetxea, X.,
525 Østergaard, O., Ostrowski, M., Park, J., Pegtel, D. M., Peinado, H., Perut, F., Pfaffl, M. W.,

526 Phinney, D. G., Pieters, B. C., Pink, R. C., Pisetsky, D. S., Pogge von Strandmann, E.,
527 Polakovicova, I., Poon, I. K., Powell, B. H., Prada, I., Pulliam, L., Quesenberry, P., Radeghieri,
528 A., Raffai, R. L., Raimondo, S., Rak, J., Ramirez, M. I., Raposo, G., Rayyan, M. S., Regev-
529 Rudzki, N., Ricklefs, F. L., Robbins, P. D., Roberts, D. D., Rodrigues, S. C., Rohde, E., Rome,
530 S., Rouschop, K. M., Rughetti, A., Russell, A. E., Saá, P., Sahoo, S., Salas-Huenuleo, E.,
531 Sánchez, C., Saugstad, J. A., Saul, M. J., Schiffelers, R. M., Schneider, R., Schøyen, T. H., Scott,
532 A., Shahaj, E., Sharma, S., Shatnyeva, O., Shekari, F., Shelke, G. V., Shetty, A. K., Shiba, K.,
533 Siljander, P. R.-M., Silva, A. M., Skowronek, A., Snyder, O. L., Soares, R. P., Sódar, B. W.,
534 Soekmadji, C., Sotillo, J., Stahl, P. D., Stoorvogel, W., Stott, S. L., Strasser, E. F., Swift, S.,
535 Tahara, H., Tewari, M., Timms, K., Tiwari, S., Tixeira, R., Tkach, M., Toh, W. S., Tomasini, R.,
536 Torrecilhas, A. C., Tosar, J. P., Toxavidis, V., Urbanelli, L., Vader, P., van Balkom, B. W., van
537 der Grein, S. G., Van Deun, J., van Herwijnen, M. J., Van Keuren-Jensen, K., van Niel, G., van
538 Royen, M. E., van Wijnen, A. J., Vasconcelos, M. H., Vechetti, I. J., Veit, T. D., Vella, L. J.,
539 Velot, É., Verweij, F. J., Vestad, B., Viñas, J. L., Visnovitz, T., Vukman, K. V., Wahlgren, J.,
540 Watson, D. C., Wauben, M. H., Weaver, A., Webber, J. P., Weber, V., Wehman, A. M., Weiss,
541 D. J., Welsh, J. A., Wendt, S., Wheelock, A. M., Wiener, Z., Witte, L., Wolfram, J., Xagorari,
542 A., Xander, P., Xu, J., Yan, X., Yáñez-Mó, M., Yin, H., Yuana, Y., Zappulli, V., Zarubova, J.,
543 Žėkas, V., Zhang, J.-Y., Zhao, Z., Zheng, L., Zheutlin, A. R., Zickler, A. M., Zimmermann, P.,
544 Zivkovic, A. M., Zocco, D., and Zuba-Surma, E. K. (2018) Minimal information for studies of
545 extracellular vesicles 2018 (MISEV2018): a position statement of the International Society for
546 Extracellular Vesicles and update of the MISEV2014 guidelines. *J Extracell Vesicles* 7, 1535750
547 13. You, Y., and Ikezu, T. (2019) Emerging roles of extracellular vesicles in
548 neurodegenerative disorders. *Neurobiol. Dis.* 130, 104512

549 14. Delpech, J.-C., Herron, S., Botros, M. B., and Ikezu, T. (2019) Neuroimmune Crosstalk
550 through Extracellular Vesicles in Health and Disease. *Trends in Neurosciences* 42, 361–372
551 15. DeLeo, A. M., and Ikezu, T. (2018) Extracellular Vesicle Biology in Alzheimer's Disease
552 and Related Tauopathy. *J Neuroimmune Pharmacol* 13, 292–308
553 16. Guo, B. B., Bellingham, S. A., and Hill, A. F. (2016) Stimulating the Release of
554 Exosomes Increases the Intercellular Transfer of Prions. *J. Biol. Chem.* 291, 5128–5137
555 17. Dinkins, M. B., Dasgupta, S., Wang, G., Zhu, G., and Bieberich, E. (2014) Exosome
556 reduction in vivo is associated with lower amyloid plaque load in the 5XFAD mouse model of
557 Alzheimer's disease. *Neurobiol. Aging* 35, 1792–1800
558 18. Bulloj, A., Leal, M. C., Xu, H., Castaño, E. M., and Morelli, L. (2010) Insulin-degrading
559 enzyme sorting in exosomes: a secretory pathway for a key brain amyloid-beta degrading
560 protease. *J. Alzheimers Dis.* 19, 79–95
561 19. Yuyama, K., Sun, H., Mitsutake, S., and Igarashi, Y. (2012) Sphingolipid-modulated
562 exosome secretion promotes clearance of amyloid-β by microglia. *J. Biol. Chem.* 287, 10977–
563 10989
564 20. Muraoka, S., DeLeo, A. M., Sethi, M. K., Yukawa-Takamatsu, K., Yang, Z., Ko, J.,
565 Hogan, J. D., Ruan, Z., You, Y., Wang, Y., Medalla, M., Ikezu, S., Chen, M., Xia, W., Gorantla,
566 S., Gendelman, H. E., Issadore, D., Zaia, J., and Ikezu, T. (2020) Proteomic and biological
567 profiling of extracellular vesicles from Alzheimer's disease human brain tissues. *Alzheimers*
568 *Dement* 16, 896–907
569 21. Muraoka, S., Lin, W., Chen, M., Hersh, S. W., Emili, A., Xia, W., and Ikezu, T. (2020)
570 Assessment of separation methods for extracellular vesicles from human and mouse brain tissues
571 and human cerebrospinal fluids. *Methods*,

572 22. McAlister, G. C., Nusinow, D. P., Jedrychowski, M. P., Wühr, M., Huttlin, E. L.,
573 Erickson, B. K., Rad, R., Haas, W., and Gygi, S. P. (2014) MultiNotch MS3 enables accurate,
574 sensitive, and multiplexed detection of differential expression across cancer cell line proteomes.
575 *Anal. Chem.* 86, 7150–7158
576 23. Elias, J. E., and Gygi, S. P. (2007) Target-decoy search strategy for increased confidence
577 in large-scale protein identifications by mass spectrometry. *Nat. Methods* 4, 207–214
578 24. Huttlin, E. L., Jedrychowski, M. P., Elias, J. E., Goswami, T., Rad, R., Beausoleil, S. A.,
579 Villén, J., Haas, W., Sowa, M. E., and Gygi, S. P. (2010) A tissue-specific atlas of mouse protein
580 phosphorylation and expression. *Cell* 143, 1174–1189
581 25. Ting, L., Rad, R., Gygi, S. P., and Haas, W. (2011) MS3 eliminates ratio distortion in
582 isobaric multiplexed quantitative proteomics. *Nat. Methods* 8, 937–940
583 26. Perez-Riverol, Y., Csordas, A., Bai, J., Bernal-Llinares, M., Hewapathirana, S., Kundu,
584 D. J., Inuganti, A., Griss, J., Mayer, G., Eisenacher, M., Pérez, E., Uszkoreit, J., Pfeuffer, J.,
585 Sachsenberg, T., Yilmaz, S., Tiwary, S., Cox, J., Audain, E., Walzer, M., Jarnuczak, A. F.,
586 Ternent, T., Brazma, A., and Vizcaíno, J. A. (2019) The PRIDE database and related tools and
587 resources in 2019: improving support for quantification data. *Nucleic Acids Res.* 47, D442–D450
588 27. Paulo, J. A., Jedrychowski, M. P., Chouchani, E. T., Kazak, L., and Gygi, S. P. (2018)
589 Multiplexed Isobaric Tag-Based Profiling of Seven Murine Tissues Following In Vivo Nicotine
590 Treatment Using a Minimalistic Proteomics Strategy. *Proteomics* 18, e1700326
591 28. Keerthikumar, S., Chisanga, D., Ariyaratne, D., Saffar, Al, H., Anand, S., Zhao, K.,
592 Samuel, M., Pathan, M., Jois, M., Chilamkurti, N., Gangoda, L., and Mathivanan, S. (2016)
593 ExoCarta: A Web-Based Compendium of Exosomal Cargo. *J. Mol. Biol.* 428, 688–692

29. Huang, D. W., Sherman, B. T., and Lempicki, R. A. (2009) Systematic and integrative analysis of large gene lists using DAVID bioinformatics resources. *Nat Protoc* 4, 44–57

30. Dennis, G., Sherman, B. T., Hosack, D. A., Yang, J., Gao, W., Lane, H. C., and Lempicki, R. A. (2003) DAVID: Database for Annotation, Visualization, and Integrated Discovery. *Genome Biol.* 4, P3

31. Sharma, K., Schmitt, S., Bergner, C. G., Tyanova, S., Kannaiyan, N., Manrique-Hoyos, N., Kongi, K., Cantuti, L., Hanisch, U.-K., Philips, M.-A., Rossner, M. J., Mann, M., and Simons, M. (2015) Cell type- and brain region-resolved mouse brain proteome. *Nat. Neurosci.* 18, 1819–1831

32. Keren-Shaul, H., Spinrad, A., Weiner, A., Matcovitch-Natan, O., Dvir-Szternfeld, R., Ulland, T. K., David, E., Baruch, K., Lara-Astaiso, D., Toth, B., Itzkovitz, S., Colonna, M., Schwartz, M., and Amit, I. (2017) A Unique Microglia Type Associated with Restricting Development of Alzheimer's Disease. *Cell* 169, 1276–1290.e17

33. Krasemann, S., Madore, C., Cialic, R., Baufeld, C., Calcagno, N., Fatimy, El, R., Beckers, L., O'Loughlin, E., Xu, Y., Fanek, Z., Greco, D. J., Smith, S. T., Tweet, G., Humulock, Z., Zrzavy, T., Conde-Sanroman, P., Gacias, M., Weng, Z., Chen, H., Tjon, E., Mazaheri, F., Hartmann, K., Madi, A., Ulrich, J. D., Glatzel, M., Worthmann, A., Heeren, J., Budnik, B., Lemere, C., Ikezu, T., Heppner, F. L., Litvak, V., Holtzman, D. M., Lassmann, H., Weiner, H. L., Ochando, J., Haass, C., and Butovsky, O. (2017) The TREM2-APOE Pathway Drives the Transcriptional Phenotype of Dysfunctional Microglia in Neurodegenerative Diseases. *Immunity* 47, 566–581.e9

34. Clayton, K. A., Van Enoo, A. A., and Ikezu, T. (2017) Alzheimer's Disease: The Role of Microglia in Brain Homeostasis and Proteopathy. *Front Neurosci* 11, 680

617 35. Vermes, I., Haanen, C., Steffens-Nakken, H., and Reutelingsperger, C. (1995) A novel
618 assay for apoptosis. Flow cytometric detection of phosphatidylserine expression on early
619 apoptotic cells using fluorescein labelled Annexin V. *J. Immunol. Methods* 184, 39–51
620 36. Benmamar-Badel, A., Owens, T., and Wlodarczyk, A. (2020) Protective Microglial
621 Subset in Development, Aging, and Disease: Lessons From Transcriptomic Studies. *Front*
622 *Immunol* 11, 430
623 37. Orre, M., Kamphuis, W., Osborn, L. M., Jansen, A. H. P., Kooijman, L., Bossers, K., and
624 Hol, E. M. (2014) Isolation of glia from Alzheimer's mice reveals inflammation and dysfunction.
625 *Neurobiol. Aging* 35, 2746–2760
626 38. Clayton, K. A., Delpech, J.-C., Herron, S., Iwahara, N., Saito, T., Saido, T. C., Ikezu, S.,
627 and Ikezu, T. (2020) Amyloid plaque deposition accelerates tau propagation via activation of
628 microglia in a humanized APP mouse model. *bioRxiv* 11, 2020.09.22.308015
629

630 **Table 1**

Protein Id	Gene Symbol	WT average	*APP/PS1* average	fold change	-log$_{10}$(*p*-value)[a]
E9Q2W9	Actn4	34.11	20.29	0.59	1.562
Q9ERF3	Wdr61	32.77	20.62	0.63	2.349
Q9EST5	Anp32b	47.50	23.84	0.50	1.812
Q9DC61	Pmpca	28.57	11.91	0.42	2.019
Q9JIZ0	Cml1	45.26	33.66	0.74	1.311
P46735	Myo1b	181.70	146.27	0.81	2.917
E9Q137	Tex264	167.37	123.23	0.74	1.527
Q62148	Aldh1a2	237.12	148.74	0.63	1.996
Q9D6J6	Ndufv2	575.30	330.89	0.58	1.413
Q8C5H8	Nadk2	153.93	131.47	0.85	1.324
P16254	Srp14	159.83	111.25	0.70	1.794
O35887	Calu	596.76	394.05	0.66	1.892
P24472	Gsta4	260.99	200.33	0.77	1.753
Q9CQN1	Trap1	131.26	98.76	0.75	1.512
Q05920	Pc	944.43	818.06	0.87	1.658
Q8BIP0	Dars2	27.08	18.13	0.67	1.895
Q6ZQK5	Acap2	811.17	944.92	1.16	1.452
P62242	Rps8	647.87	897.33	1.39	1.536
P62301	Rps13	600.46	848.51	1.41	1.364
Q8BT60	Cpne3	1068.06	1156.14	1.08	1.351
P39447	Tjp1	124.75	156.82	1.26	1.990
Q61730	Il1rap	1109.54	1283.78	1.16	1.371
P48036	Anxa5	2756.53	3220.07	1.17	1.693
Q921E2	Rab31	93.36	121.57	1.30	1.387
P14824	Anxa6	3667.05	4291.27	1.17	1.467
P58021	Tm9sf2	321.28	416.33	1.30	1.364
P05067-4	APP	1441.70	3198.42	2.22	2.850
P49768	PSEN1	229.33	382.95	1.67	4.245
Q91VU0	Fam3c	103.78	141.34	1.36	1.439
Q99PD7	Slc24a3	59.07	79.27	1.34	1.524
Q9CQJ6	Denr	26.78	36.86	1.38	1.710
Q9JJC6	Rilpl1	22.97	30.63	1.33	1.476
Q80TL7	Mon2	103.59	129.03	1.25	1.681
Q3B7Z2	Osbp	370.13	474.24	1.28	1.308
Q9QXH4	Itgax	29.00	78.77	2.72	2.291
Q8C7N7	Aph1b	69.45	102.88	1.48	1.993
P06800	Ptprc	143.06	210.96	1.47	1.636
P20491	Fcer1g	86.16	127.79	1.48	1.455
Q9CPV9	P2ry12	2248.44	2808.41	1.25	1.613
P60766	Cdc42	844.66	932.37	1.10	0.370
Q80UP3	Dgkz	167.80	207.27	1.24	1.670
P62192	Psmc1	1531.69	1674.17	1.09	1.746
Q5SYD0	Myo1d	1717.22	2076.67	1.21	1.350
A2ADY9	Ddi2	84.14	104.29	1.24	2.941
A2AF47	Dock11	198.13	296.61	1.50	1.329
Q8BIK4-2	Dock9	725.87	1049.00	1.45	1.415

631 [a]The t.test was calculated by Welch's test.
632
633
634

635

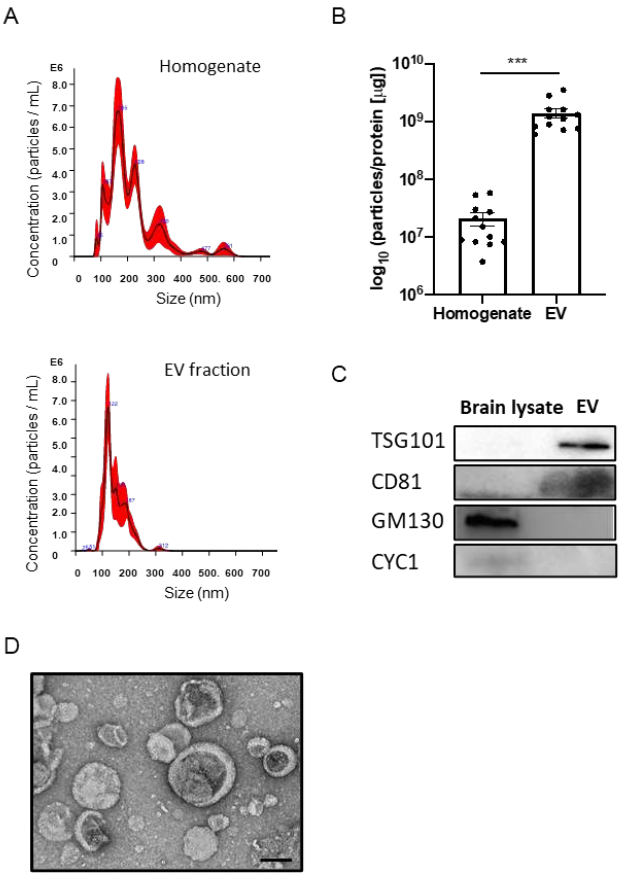

636

637 **Figure 1. Biochemical characteristic of brain-derived EVs separated from frozen mouse**
638 **brain tissue: A)** NTA plot of average size and concentration of particles from brain
639 homogenates and separated EV fraction. The black line shows the fitting curve. Red line
640 represents the error bar. The y axis is the concentration of particles. The x axis is the size of
641 particle. Top: brain homogenates, Bottom: separated EV fraction. **B)** The ratio of particles to
642 protein concentration to quantify particle purity ($p = 0.005$ by paired samples Wilcoxon test). **C)**
643 Assessment of EV and non-EV marker protein, including TSG101, CD81, GM130 (Golgi
644 marker), CYC1 (Mitochondrial marker) in separated EV fraction. **D)** Transmission electron
645 microscopy (TEM) image of mouse brain-derived EV fraction. Scale bar; 100 nm.

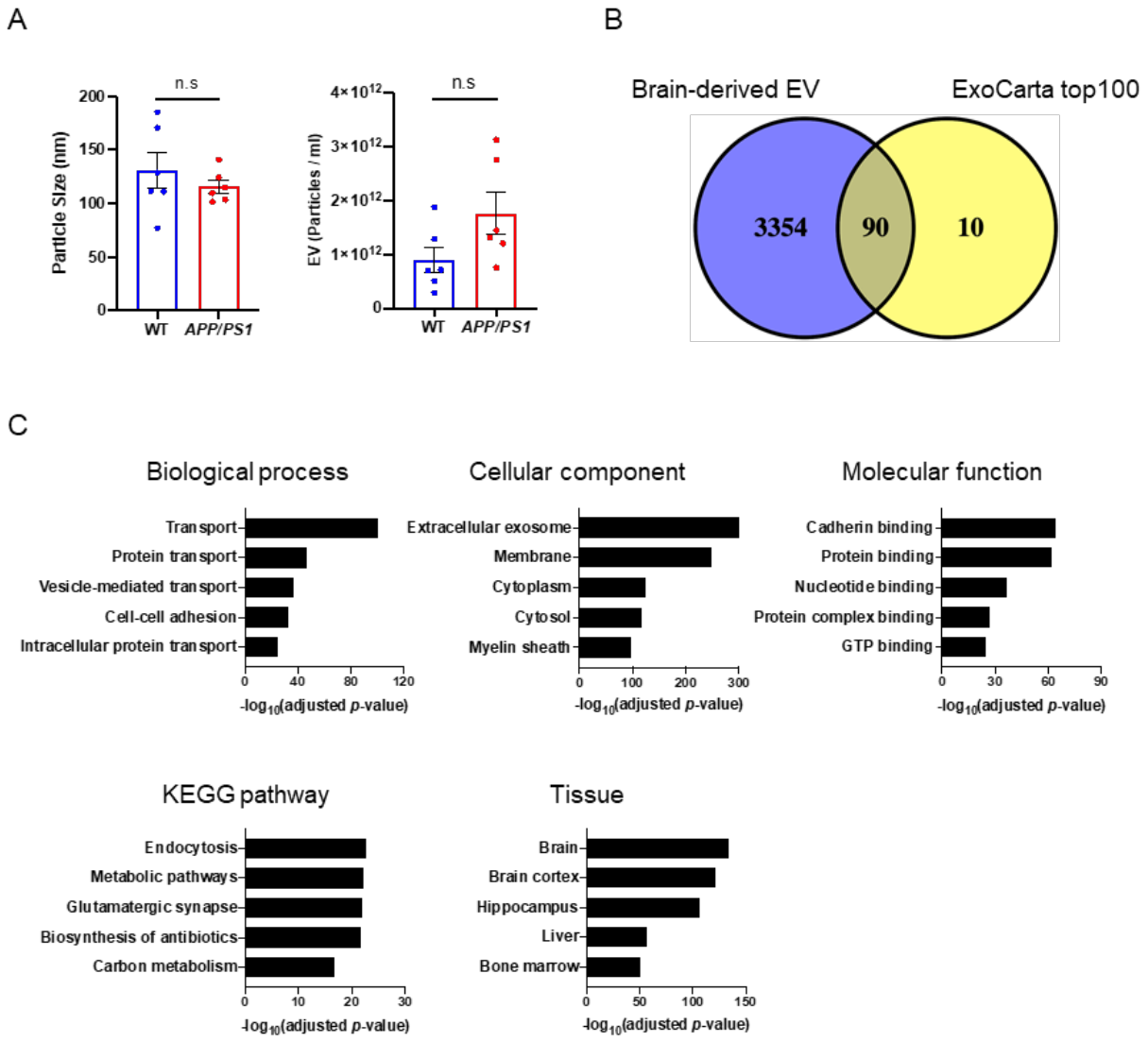

646

647 **Figure 2. Proteomic profiling of mouse brain-derived EV: A)** Comparison of particle number
648 and size in EV fraction separated from CAST.*APP/PS1* and WT mouse brain tissue. Left:
649 particle size, Right: particle number. **B)** Venn diagram representing the proteins identified in
650 brain-derived EV and ExoCarta top100. **C)** DAVID GO analysis using DAVID Bioinformatics
651 Resources 6.8. The GO term of Top5 Biological Process, Cellular Component, Molecular
652 Function, KEGG pathway and Tissue ontology with -$\log_{10}$ (FDR *p*-value).

653

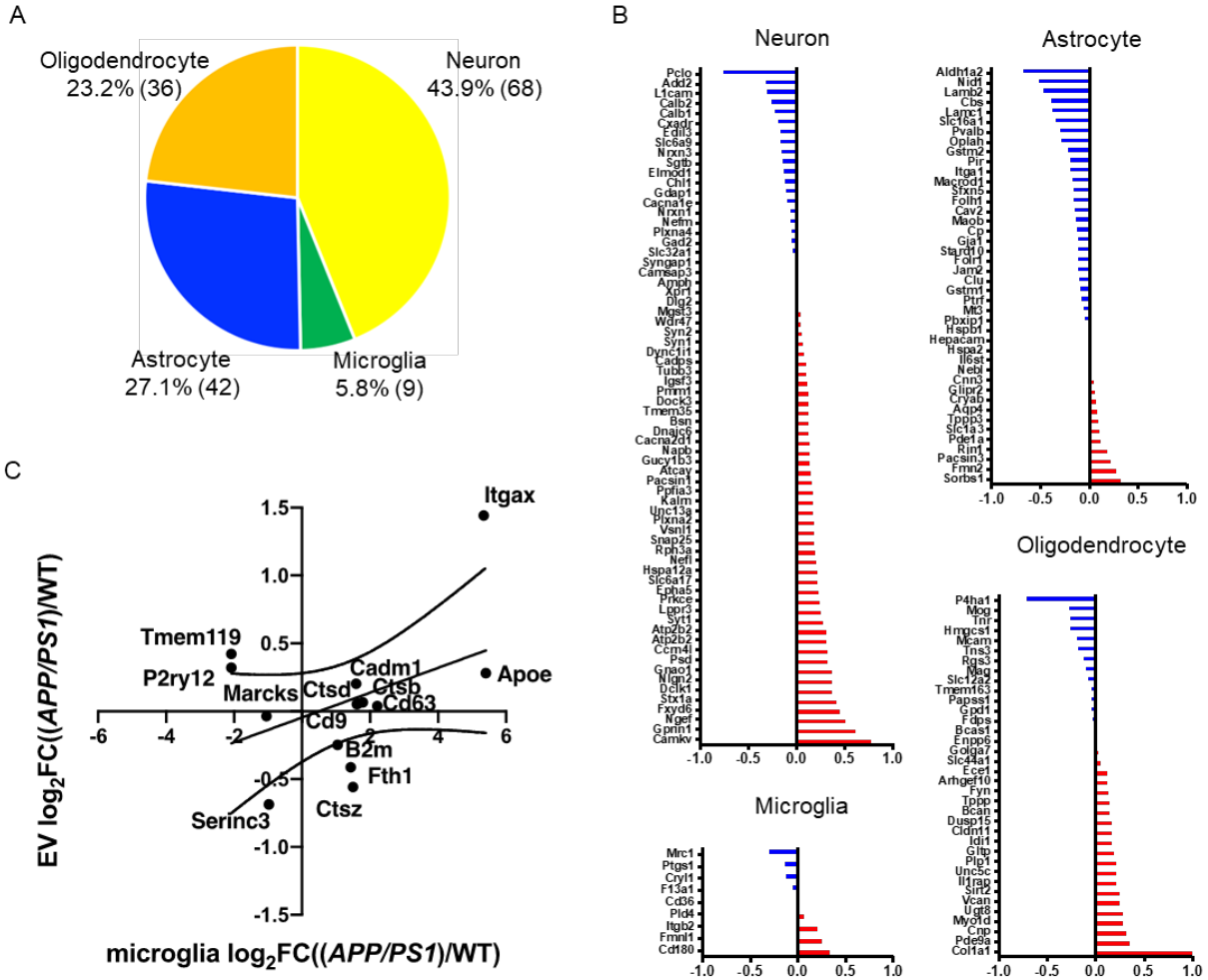

654

655 **Figure 3. Cell type-specific proteins comparison of CAST. *APP/PS1* and WT mouse brain-**
656 **derived EV: A)** Enrichment of brain cell type-specific markers in brain-derived EV proteins.
657 Yellow: Neuron, Green: Microglia, Blue: Astrocytes, Orange: Oligodendrocytes. The
658 parentheses show the number of identified cell type-specific proteins. **B)** Comparison of the cell
659 type-specific protein in CAST.*APP/PS1*-derived EVs and CAST WT EVs. The red bar shows
660 higher expression in *APP/PS1* compared with WT and Blue bar indicates higher expression in
661 WT compared with *APP/PS1*. **C)** Comparison of $\log_2$ fold change of the differential expression
662 of DAM versus homeostatic microglia in the 5xFAD (x axis) to the $\log_2$ fold change of the
663 differential expression of CAST.*APP/PS1* versus WT (y axis).

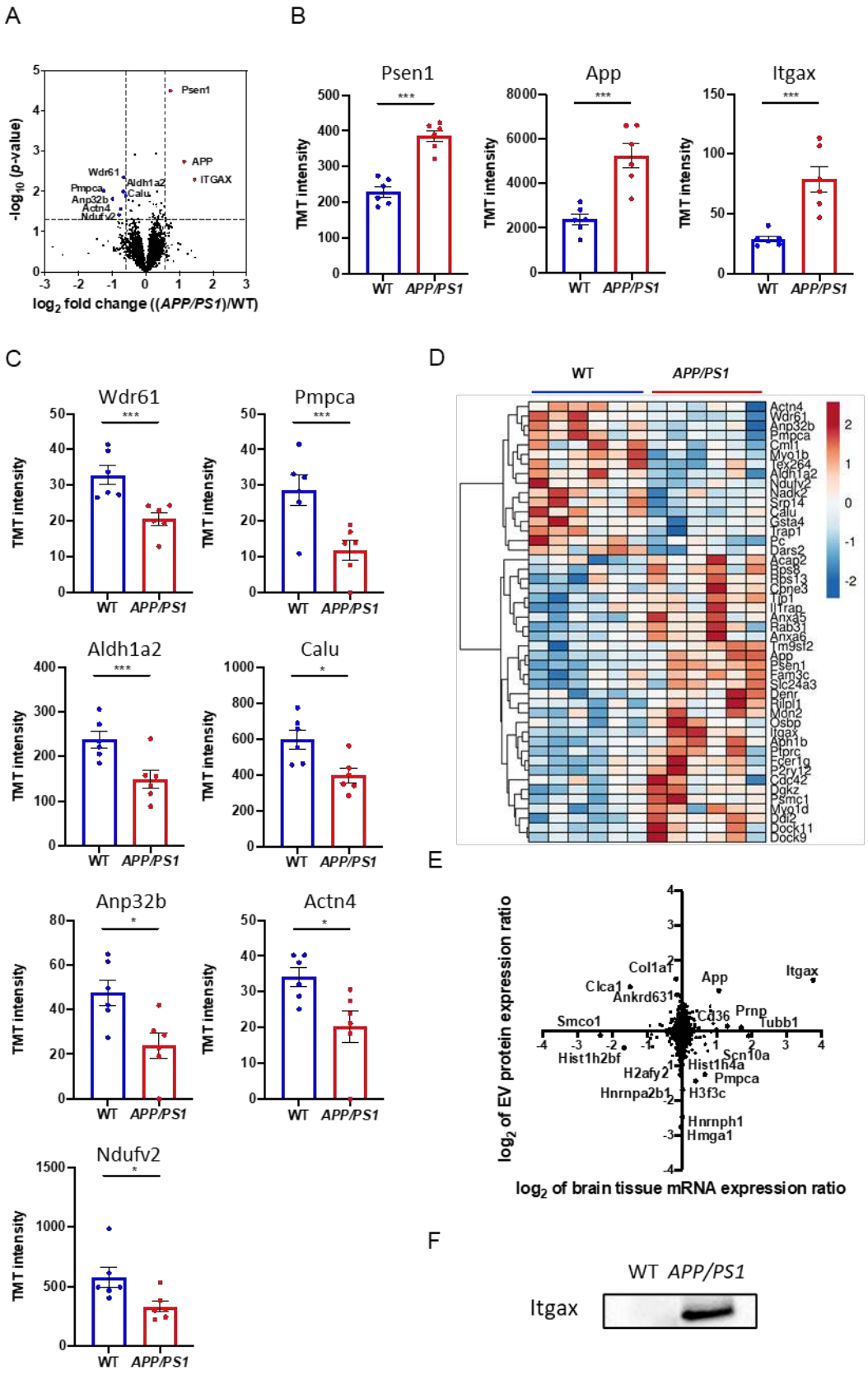

664

Figure 4. Comparison of CAST.*APP/PS1* brain-derived EV and CAST WT EV: A) Volcano plot showing degree of differential expression of brain-derived EV proteins in AAP/PS1 compared with WT. The x-axis indicates $\log_2$ transformed fold change in expression. The y-axis shows $-\log_{10}$ transformed *p*-values. The grey dot line shows the 1.3010 $-\log_{10}$(*p*-value) cutoff and 0.585 or -0.585 $\log_2$FC cutoff. **B, C)** A scatter plot of TMT reporter ion intensity as measured by proteomics per selected candidate protein. The t.test was calculated by Welch's test. **B)** The three proteins were up-regulated in *APP/PS1* compared to WT. Psen1: $-\log_{10}$(*p*-value) = 4.245, FC = 1.67, App: $-\log_{10}$(*p*-value) = 2.850, FC = 2.22, Itgax: $-\log_{10}$(*p*-value) = 2.291, FC = 2.72. **C)** The 7 proteins were down-regulated in *APP/PS1* compared to WT. Wdr61: $-\log_{10}$(*p*-value) = 2.349, FC = 0.63, Pmpca: $-\log_{10}$(*p*-value) = 2.019, FC = 0.42, Aldh1a2: $-\log_{10}$(*p*-value) = 1.996, FC = 0.63, Calu: $-\log_{10}$(*p*-value) = 1.892, FC = 0.66, Anp32b: $-\log_{10}$(*p*-value) = 1.812, FC = 0.50, Actn4: $-\log_{10}$(*p*-value) = 1.562, FC = 0.59 and Ndufv2: $-\log_{10}$(*p*-value) = 1.413, FC = 0.58. **D)** Heatmap of 46 proteins with the 1.3010 $-\log_{10}$(*p*-value) cutoff. The value shows $\log_2$(FC). **E)** Comparison of protein expression and mRNA expression in *APP/PS1* and WT. The y axis is the ratio of EV protein expression. The x axis is the ratio of brain tissue mRNA expression. The Spearman rank correlation coefficient (rho) shows 0.06709 (p = 0.0001). F) Validation of Itgax in separated EV fraction from CAST.*APP/PS1* and WT mouse brain tissue using Western blot.